Steel and Composite Structures, *Vol. 36, No. 6 (2020) 711-727*
DOI: https://doi.org/10.12989/scs.2020.36.6.711

Free vibration of FG-GPLRC spherical shell on two parameter elastic foundation

Arameh Eyvazian[1,2], Farayi Musharavati[3], Pouyan Talebizadehsardari*[4,5] and Tamer A. Sebaey[6,7]

[1]Institute of Research and Development, Duy Tan University, Da Nang 550000, Vietnam
[2]Faculty of Electrical – Electronic Engineering, Duy Tan University, Da Nang 550000, Vietnam
[3]Department of Mechanical and Industrial Engineering, College of Engineering, Qatar University, P.O. Box 2713, Doha, Qatar
[4]Metamaterials for Mechanical, Biomechanical and Multiphysical Applications Research Group, Ton Duc Thang University, Ho Chi Minh City, Vietnam
[5]Faculty of Applied Sciences, Ton Duc Thang University, Ho Chi Minh City, Vietnam
[6]Engineering Management Department, College of Engineering, Prince Sultan University, Riyadh, Saudi Arabia
[7]Mechanical Design and Production Department, Faculty of Engineering, Zagazig University, P.O. Box 44519, Zagazig, Sharkia, Egypt

(*Received December 8, 2019, Revised April 4, 2020, Accepted August 24, 2020*)

Abstract. In the present research, the free vibration analysis of functionally graded (FG) nanocomposite deep spherical shells reinforced by graphene platelets (GPLs) on elastic foundation is performed. The elastic foundation is assumed to be Winkler-Past ernak-type. It is also assumed that graphaene platelets are randomly oriented and uniformly dispersed in each layer of the nanocomposite shell. Volume fraction of the graphene platelets as nanofillers may be different in the layers. The modified HalpinTsai model is used to approximate the effective mechanical properties of the multilayer nanocomposite. With the aid of the first order shear deformation shell theory and implementing Hamilton's principle, motion equations are derived. Afterwards, the generalized differential quadrature method (GDQM) is utilized to study the free vibration characteristics of FG-GPLRC spherical shell. To assess the validity and accuracy of the presented method, the results are compared with the available researches. Finally, the natural frequencies and corresponding mode shapes are provided for different boundary conditions, GPLs volume fraction, types of functionally graded, elastic foundation coefficients, opening angles of shell, and thickness-to-radius ratio.

Keywords: spherical shell; graphene platelets; GDQM; nanocomposite

1. Introduction

A novel nanostructures of carbon which is a single atomic and two-dimensional layer has discovered in 2004 (see Novoselov *et al*. 2004) and named graphene. The graphene structure includes the atoms joined through bundles. Owing to its superior thermal, electrical and mechanical properties, graphene has attracted the attention of scientists. Owing to its superior thermal, electrical and mechanical properties, graphene has attracted the attention of scientists. Therefore, numerous studies (Reddy *et al.* 2006, Scarpa *et al*. 2009, cadelano *et al.* 2009, zhang et al. 2011) have been conducted to explore the extraordinary features of graphene. In the present paper and many other available works, the potential of graphene as a promising nano-fillers for the composites is highlighted.

Graphene layer exhibits higher stiffness compared to most of the engineering and industrial metals such as stainless steel. The Young's modulus of this nanostructure has been reported as 1TPa. Graphene presents privileged conduction capacity even more than copper and silver. Other characteristics of graphene are mentioned in (Stankovich *et al*. 2006, Potts *et al.* 2011). It is also observed that, addition of a small quantity of graphene as reinforcement in a nanocomposite media can result in better mechanical, thermal and electrical properties (Rafiee *et al.* 2009, Zhao *et al*. 2010). Owing to its flat structure, in many applications, graphene is preferred compared with most of nanocomposites based on carbon nanotubes because of the better interacting of the graphene with polymer.

Based on several experimental works, the natural frequency of the nanocomposites could be remarkably enhanced by incorporation of graphene nanofillers even at low weight fractions. For instance Chandra *et al*. (2012) reported the enhanced natural frequencies of a composite media by adding graphene fillers. According to the theoretical analysis, it is verified that the natural frequencies of the graphene-embedded nanocomposites are much higher than the graphene-free matrix. For instance, Song et al. (2017) expressed that introducing only 1.2% graphene weight fraction leads to increase natural frequency about 160%. In another work, Rafiee et al. (2009) reported that incorporation of 0.1 (w.t.%) of GPLs, the strength and stiffness of the reinforced polymer composites are enhanced by the same amount attain by adding 1.0 w.t.% of carbon nanotubes (CNTs). It should be noted that, the weight fraction of grpahene reinforcement cannot be augmented arbitrarily as over-addition of graphene nanofillers may results in unpleasant effects (Kulkarni *et al*. 2010).

∗Corresponding author, Ph.D.
E-mail: ptsardari@tdtu.edu.vn

http://www.techno-press.org/?journal=scs&subpage=8
ISSN: 1229-9367 (Print), 1598-6233 (Online)

Graphene nanofiller is apperceived in two type; i.e., graphene sheets (GRC) and graphene platelets (GPLRC). Thermo-mechanical characteristics are procured based on a refined micro-mechanical rule that is calibrated using the obtained information of molecular dynamics simulations. The weight fraction of graphene sheets in the first model varies between 3-11 percent and constituents are assumed temperature dependent. Vibrational analysis of thin structures reinforced with graphene sheets has been well documented in the open literature. When composites are reinforced with graphene sheets, Wang *et al*. (2019) analyzed free vibration of graphene reinforced composite beams based on the plane-stress state in each layer. A hybrid Kantorovich-Galerkin method is applied to this problem. FG-GRC Beams resting on elastic foundation are investigated by Shen *et al.* (2017a) considering a thermal environment. Also, Shen *et al*. (2019a) explored the nonlinear vibration of post-buckled nanocomposite beam based on the von Kármán strain-displacement relationships. Large amplitude vibration of functionally graded reinforced composite plates are addressed by shen *et al*. (2019b) when they are subjected to thermal load with temperature-dependent material properties with and without considering elastic foundation (Shen *et al.* 2019c, Shen *et al.* 2017b). NURBS based isogeometric finite element method is utilized to investigate the nonlinear free vibration of FG-GRC plates by Kiani (2018). Using the mentioned method this Author examined the post-buckling of a FG-GPLRC plate (see Kiani and Mirzaei 2019). The effects of thermal environment on natural frequency are presented. Shen et al. (2017c, 2018) analyzed vibration behavior of cylindrical shells and panels applying two step perturbation method. Influences of Graphene sheet volume fraction and piece-wise pattern on fundamental frequency are studied.

In another novel class, graphene platelets are assumed as reinforcement in the matrix of the nanocomposite media. In this type of reinforced composites, properties are calculated considering the Halpin-Tsai micromechanical rule. The weight fraction of grpahene platelets in this model is less that 1 percent and properties are assumed to be temperature-independent. The main researches on the vibration response of nano structures reinforced with graphene platelets are as follows: Kitipornchai *et al.* (2017) obtained non-dimensional frequencies of porous nanocomposite beams using Ritz method. Also, based on the Ritz technique, the nonlinear free vibration of FG-GPLRC beams are investigated by Feng *et al.* (2017). Vibration responses of the graphene platelets-embedded nanocomposite beams subjected two successive moving masses are determined by Wang *et al*. (2019). Equations of motion are governed implementing a new higher order shear deformation theory and are solved using Hybrid Navier-Newmark solution. Vibration Characteristic of curved porous FG-GPL nanocomposite beams are studied by Anirudh *et al*. (2019). Vibration response of FG-GPLRC plate are studied by Song *et al*. (2017) for the first time using Navier method. Zhao *et al.* (2017) conducted a theoretical study on the free vibration of functionally graded trapezoidal plates reinforced with graphene nanoplatelets. Gua *et al*. (2018) employed IMLS-Ritz approximation to investigate the free vibration of functionally graded quadrilateral nanocomposite plates reinforced by graphene platelets filler. In the mentioned study, the effective material properties were determined by the modified Halpin-Tsai model and rule of mixture. The nonlinear forced (see Gholami and Anari 2018) and free (see Gao *et al.* 2018) vibration analysis of FG-GPLRC rectangular plates were also addressed in the literature. Gholami and Ansari (2019) explored the free vibration response applying a novel differential quadrature method based on the energy functional of nanocomposites embedded by graphene platelets. Transformed differential quadrature method is used to obtain the natural frequencies and corresponding mode shapes of an FG-GPLRC eccentric annular plate (Malekzadeh *et al.* 2018). In this paper, the frequencies are controlled by two piezoelectric layers which are located on the top and bottom of plate. Moreover, Saidi *et al*. (2019) employed Galerkin method to analyze the vibration behavior FG-GPLRC plate surrounded by two piezoelectric layers. Furthermore, the effect of supersonic flow on the natural frequency are investigated. Thai *et al*. (2019) performed a comprehensive study to analyze functionally graded GPLRC plate utilizing NURBS formulation. Dong *et al.* (2018) presented the nonlinear free vibration analysis of FG-GPLRC cylindrical shells with spinning motion. Implementing an analytical method and based on the three dimensional elasticity, Liu *et al*. (2018) examined the free vibration of an initially stressed functionally graded graphene platelets reinforced composite cylindrical shells. Wang *et al*. (2018) analyzed the free vibration of simply-supported doubly curved shallow nanocomposite shells reinforced by graphene nanoplatelets.

As the above literature survey reveals, numerous investigations are available on nanocomposite structures reinforced by graphene platelets. However, the free vibration analysis of spherical shells has not been addressed. In this regard, the current research applied the first order shear deformation shell theory to analyze the free vibration behavior of spherical shell. Furthermore, the solution method is based on the generalized differential quadrature method suitable for arbitrary boundary conditions. In the present investigation, natural frequencies of multi-layer graphene platelet reinforced composite spherical shells with and without hole in the apex of shell are determined. Also, the shell is assumed on the pasternak-type elastic foundation. Various patterns of functionally graded for graphene reinforcements is assumed into the formulation. Halpin-Tsai micromechanical rule and the Hamilton's principle are used to obtain the motion equations dealing with the vibration of FG-GPLRC shell on elastic foundation. The influence of different parameters are investigated on the natural frequencies and mode shape for free vibration phenomena.

2. Geometry and material properties of spherical shell

Consider a FG-GPLRC laminated spherical shell of uniform thickness h in total domain and radius of curvature R. The spherical shell domain is bounded by $\varphi_{in} \le \varphi \le \varphi_{out}$, $0 \le \theta \le 2\pi$, and $-h/2 \le z \le h/2$ with respect to the coordinates φ, θ and z along the meridional, circumferential and radial directions. The coordinates system (φ, θ, z) with its origin located at the mid-surface center of the shell is defined, as shown in Fig. 1.

In this paper, the multilayer graphene nanocomposite spherical shell is considered with perfectly bonded GPLRC layers of the equal thicknesses. Each ply is made from a mixture of GPL filler and isotropic polymer matrix in which GPLs are randomly oriented and uniformly dispersed. Therefore, the nanoplatelets volume fraction may have a step layer-wise variation along the thickness.

It is supposed that the composite laminated shell includes even number of layers, N_L. Four different types of volume fraction are assumed in this study for FG-GPLRCs (see Wu *et al*. 2017): FG-O, FG-X, FG-Λ, and UD. In the uniform distribution (UD), the GPL constituent remains constant across all the layers, thus U-GPLRC correlate with an isotropic homogeneous shell. In the step functionally graded distributions, the GPL volume fraction linearly varies from layer to layer. For the case of X-GPLRC, the top and bottom layers are nanoplatelet rich while this is inversed for O-GPLRC where the middle layers are rich in GPL filler. Eventually, Λ-GPLRC is an asymmetrical repartition where nanofillers volume fraction linearly increase from the top to the bottom layers. Distribution of volume fraction for each layer fits in the following expressions (see Wu *et al*. 2017)

$$\mathrm{U-GPLRC} \ : \ V_{GPL}^{(k)} = V_{GPL}^{*}$$

$$\mathrm{X-GPLRC} \ : \ V_{GPL}^{(k)} = 2V_{GPL}^{*}|2k - N_L - 1|/N_L$$

$$\mathrm{O-GPLRC} \ : \ V_{GPL}^{(k)} = 2V_{GPL}^{*}(1 - |2k - N_L - 1|/N_L)$$

$$\Lambda-\mathrm{GPLRC} \ : \ V_{GPL}^{(k)} = V_{GPL}^{*}(2k-1)/N_L \tag{1}$$

where, $V_{GPL}^{(k)}$ illustrates the volume fraction of GPLs in the k-th layer of the laminate. In Eq. (1) k takes the amount from 1 to N_L. Also V_{GPL}^{*} displays the total volume fraction of the graphene platelets in the deep spherical shell. The total volume fraction of GPLs may be represented in terms of the weight fraction of the GPLs in the whole shell, W_{GPL} and also the mass density of the constituents, ρ_m and ρ_{GPL} are as follow

$$V_{GPL}^{*} = \frac{W_{GPL}}{W_{GPL} + \left(\frac{\rho_{GPL}}{\rho_m}\right)(1 - W_{GPL})} \tag{2}$$

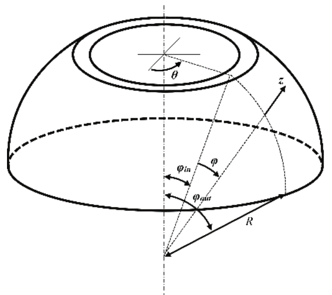

Fig. 1 Schematic and coordinate system for a spherical shell

It is known that in the graphene-based nanocomposites the size and geometry of the nanoplatelets are two important factors for estimation of properties of polymer composites. To compute the effective elasticity modulus of the GPLRCs in this research, the Halpin-Tsai rule is utilized. This rule is widely accepted for determination of effective elasticity modulus of GPLRCs (Affdl and Kardos, 1976). According to this micromechanical rule, the elasticity modulus of each layer of the composite can be obtained taking into account the nanofillers' geometry and dimension as follow

$$E^{(k)} = \frac{3}{8}\frac{1 + \xi_L\eta_L V_{GPL}^{(k)}}{1 - \eta_L V_{GPL}^{(k)}} \times E_m + \frac{5}{8}\frac{1 + \xi_T\eta_T V_{GPL}^{(k)}}{1 - \eta_T V_{GPL}^{(k)}} \times E_m \tag{3}$$

where the subsidiary parameters η_L and η_T in Eq. (3) are expressed as

$$\eta_L = \frac{\left(\frac{E_{GPL}}{E_m}\right) - 1}{\left(\frac{E_{GPL}}{E_m}\right) + \xi_L}, \qquad \eta_T = \frac{\left(\frac{E_{GPL}}{E_m}\right) - 1}{\left(\frac{E_{GPL}}{E_m}\right) + \xi_T} \tag{4}$$

In Eq. (4), E_m and E_{GPL} are the Young's modulus of the isotropic matrix and GPLs, respectively. The geometrical factors of GPLs can be obtained in terms of the thickness of the GPLs, t_{GPL}, width of the GPLs, b_{GPL} and length of the GPLs, a_{GPL} as follows

$$\xi_L = 2\left(\frac{a_{GPL}}{t_{GPL}}\right), \qquad \xi_T = 2\left(\frac{b_{GPL}}{t_{GPL}}\right) \tag{5}$$

The effective Poisson's ratio of the composite media ν and The mass density of the composite media ρ may be easily obtained by means of the properties of the constituents according to the Voigt rule of mixtures. Accordingly one may write

$$\begin{aligned} \rho^{(k)} &= \rho_{GPL}V_{GPL}^{(k)} + \rho_m V_m^{(k)} \\ \nu^{(k)} &= \nu_{GPL}V_{GPL}^{(k)} + \nu_m V_m^{(k)} \end{aligned} \tag{6}$$

In Eq. (6), the subscripts m and GPL show the matrix and graphene platelets nanofiller, respectively. $V_m = 1 - V_{GPL}$ is the isotropic polymer volume fraction.

3. Theoretical formulations

Based on the first order shear deformation theory (FSDT) assumptions, the displacements field (u_1, u_2, u_3) of an arbitrary supposed point in the composite media of spherical shell are exhibited in terms of the displacements and rotations of the reference surface

$$u_1(\varphi,\theta,z,t) = u_1^0(\varphi,\theta,t) + z\psi_1(\varphi,\theta,t)$$

$$u_2(\varphi,\theta,z,t) = u_2^0(\varphi,\theta,t) + z\psi_2(\varphi,\theta,t)$$

$$u_3(\varphi,\theta,z,t) = u_3^0(\varphi,\theta,t) \tag{7}$$

where u_1^0, u_2^0, and u_3^0 illustrate the displacements of the reference surface $(z = 0)$ in the φ, θ, and z directions, respectively; Moreover, ψ_1 and ψ_2 denote the transverse normal rotations of the reference surface about the θ and φ axes, respectively. Also, t is the time variable.

Strain components associated with the displacements field (7), according to the assumed shell theory, may be expanded in vector forms as (Reddy 2006)

$$\{\varepsilon\} = \{\varepsilon^0\} + z\{\varepsilon^1\} \tag{8}$$

where

$$\begin{Bmatrix} \varepsilon_1^0 \\ \varepsilon_2^0 \\ \varepsilon_4^0 \\ \varepsilon_5^0 \\ \varepsilon_6^0 \end{Bmatrix} = \left(1+\frac{z}{R}\right)^{-1} \times \begin{Bmatrix} \frac{1}{R}\left(u_{1,\varphi}^0 + u_3^0\right) \\ \frac{1}{R\sin(\varphi)}\left(u_{2,\theta}^0 + \cos(\varphi)u_1^0 + \sin(\varphi)u_3^0\right) \\ \frac{1}{R}\left(\frac{1}{\sin(\varphi)}u_{3,\theta}^0 - u_2^0 + R\psi_2\right) \\ \frac{1}{R}\left(u_{3,\varphi}^0 - u_1^0 + R\psi_1\right) \\ \frac{1}{R}\left(u_{2,\varphi}^0\right) + \frac{1}{R\sin(\varphi)}\left(u_{1,\theta}^0 - \cos(\varphi)u_2^0\right) \end{Bmatrix} \tag{9}$$

$$\begin{Bmatrix} \varepsilon_1^1 \\ \varepsilon_2^1 \\ \varepsilon_4^1 \\ \varepsilon_5^1 \\ \varepsilon_6^1 \end{Bmatrix} = \left(1+\frac{z}{R}\right)^{-1} \times \begin{Bmatrix} \frac{1}{R}\left(\psi_{1,\varphi}\right) \\ \frac{1}{R\sin(\varphi)}\left(\psi_{2,\theta} + \cos(\varphi)\psi_1\right) \\ 0 \\ 0 \\ \frac{1}{R}\left(\psi_{2,\varphi}\right) + \frac{1}{R\sin(\varphi)}\left(\psi_{1,\theta} - \cos(\varphi)\psi_2\right) \end{Bmatrix} \tag{10}$$

where ϵ_1^0, ϵ_2^0, and ϵ_6^0 are the membrane strains of the middle surface; ϵ_1^1, ϵ_2^1, and ϵ_6^1 explain the curvature changes of the spherical shell; ϵ_4^0, ϵ_5^0 indicate the transverse shear strains. The value $R(1+\frac{z}{R})$ is the Lamé parameter.

Considering linear elastic material (The Hook law), the constitutive law for each layer of the FG-GPLRC spherical shell becomes (Kar and Panda 2015)

$$\begin{Bmatrix} \sigma_1 \\ \sigma_2 \\ \sigma_4 \\ \sigma_5 \\ \sigma_6 \end{Bmatrix}^{(k)} = \begin{bmatrix} Q_{11} & Q_{12} & 0 & 0 & 0 \\ Q_{12} & Q_{22} & 0 & 0 & 0 \\ 0 & 0 & Q_{44} & 0 & 0 \\ 0 & 0 & 0 & Q_{55} & 0 \\ 0 & 0 & 0 & 0 & Q_{66} \end{bmatrix}^{(k)} \begin{Bmatrix} \varepsilon_1 \\ \varepsilon_2 \\ \varepsilon_4 \\ \varepsilon_5 \\ \varepsilon_6 \end{Bmatrix} \tag{11}$$

In the above equations, Q_{ij}'s $(i,j = 1,2,4,5,6)$ are the reduced material stiffness coefficients which are obtained as

$$Q_{11}^{(k)} = Q_{22}^{(k)} = \frac{E^{(k)}}{1-\nu^{(k)2}}, \qquad Q_{12}^{(k)} = \frac{\nu^{(k)}E^{(k)}}{1-\nu^{(k)2}}$$

$$Q_{66}^{(k)} = \frac{E^{(k)}}{2(1+\nu^{(k)})}, \qquad Q_{44}^{(k)} = Q_{55}^{(k)} = \kappa Q_{66}^{(k)} \tag{12}$$

where κ is the shear correction factor of FSDT and in general, it depends on the geometry, material properties and loading conditions where the approximate values of $\kappa = 5/6$ or $\kappa = \pi^2/12$ are used extensively (see Reddy 2006). In this work, the shear correction factor is chosen $\kappa = 5/6$. The stress resultants of the deep spherical shell are expressed in terms of the stresses components through the thickness, based on the first order theory, may be obtained as the follow form

$$(N_{11}, N_{22}, N_{12}) = \sum_{k=1}^{N_L} \int_{z_k}^{z_{k+1}} \left(1+\frac{z}{R}\right)(\sigma_1, \sigma_2, \sigma_6)^{(k)} dz$$

$$(M_{11}, M_{22}, M_{12}) = \sum_{k=1}^{N_L} \int_{z_k}^{z_{k+1}} z\left(1+\frac{z}{R}\right)(\sigma_1, \sigma_2, \sigma_6)^{(k)} dz$$

$$(Q_1, Q_2) = \sum_{k=1}^{N_L} \int_{z_k}^{z_{k+1}} \left(1+\frac{z}{R}\right)(\sigma_5, \sigma_4)^{(k)} dz \tag{13}$$

in which N_{11}, N_{22}, and N_{12} are the membrane stress resultants, M_{11}, M_{22}, and M_{12} are the bending stress resultants and Q_1 and Q_2 indicate the membrane out-of-plane shear stress resultants.

Derivation of the equations of motion of the functionally graded graphene platelets reinforced composite spherical shell is accomplished by employing Hamilton's principle. According to this principle, the motion equations of shell on the elastic foundation are derived when the following equation holds (Reddy 2006, Akbarov *et al.* 2016)

$$\int_{t_1}^{t_2} (\delta T - \delta V - \delta U)dt = 0 \tag{14}$$

In the above equation δT, δU, and δV show the first variation of the kinematic, strain and potential energy of the applied load, respectively. The strain energy δU for the composite media takes the following form

$$\delta U = \int_0^{2\pi} \int_{\varphi_{in}}^{\varphi_{out}} \int_{-0.5h}^{+0.5h} \sigma_i \delta\varepsilon_i \left(1+\frac{z}{R}\right)^2 \times R^2 \sin(\varphi)\, dz\ d\varphi\ d\theta, \qquad i = 1,2,4,5,6 \tag{15}$$

Potential energy δV due to the Winkler-Pasternak elastic foundation for the spherical shell are obtained as (Ansari 2016)

$$\delta V = \int_0^{2\pi} \int_{\varphi_{in}}^{\varphi_{out}} \left[k_w u_3^0 \delta u_3^0 + \frac{k_g}{R^2} u_{3,\varphi}^0 \delta u_{3,\varphi}^0 + \frac{k_g}{R^2 \sin^2(\varphi)} u_{3,\theta}^0 \delta u_{3,\theta}^0\right] R^2 \sin(\varphi)\ d\varphi\ d\theta \tag{16}$$

where k_w and k_g are Winkler and Pasternak coefficients of elastic foundation. Furthermore, kinetic energy is expressed as

$$\delta T = \int_0^{2\pi}\int_{\varphi_{in}}^{\varphi_{out}}\int_{-0.5h}^{+0.5h}\rho\begin{pmatrix}\dot{u}_1\delta\dot{u}_1+\dot{u}_2\delta\dot{u}_2\\ +\dot{u}_3\delta\dot{u}_3\end{pmatrix}\times \left(1+\frac{z}{R}\right)^2 R^2\sin(\varphi)\ dz\ d\varphi\ d\theta \tag{17}$$

where ρ is the mass density, which obtained from Eq. (6) for each layer. Also, a ($\dot{}$) denotes the derivative with respect to time. Substituting the stress tensor components from Eq. (11) into (15) and implementing the variational approach, the motion equations of the FG-GPLRC spherical shells resting on two parameter elastic foundation are found to be

$$\delta u_1^0 \quad : \quad \frac{1}{R}\left\{\cot(\varphi)(N_{11}-N_{22})+N_{11,\varphi}+\frac{1}{\sin(\varphi)}N_{12,\theta}+Q_1\right\}=I_1\ddot{u}_1^0+I_2\ddot{\psi}_1$$

$$\delta u_2^0 \quad : \quad \frac{1}{R}\left\{2\cot(\varphi)N_{12}+N_{12,\varphi}+\frac{1}{\sin(\varphi)}N_{22,\theta}+Q_2\right\}=I_1\ddot{u}_2^0+I_2\ddot{\psi}_2$$

$$\delta u_3^0 \quad : \quad \frac{1}{R}\left\{\cot(\varphi)Q_1+Q_{1,\varphi}+\frac{1}{\sin(\varphi)}Q_{2,\theta}-(N_{11}+N_{22})-k_wR^2u_3^0+k_g\cot(\varphi)u_{3,\varphi}^0+k_gu_{3,\varphi\varphi}^0+k_g\frac{1}{\sin^2(\varphi)}u_{3,\theta\theta}^0\right\}=I_1\ddot{u}_3^0$$

$$\delta\psi_1 \quad : \quad \frac{1}{R}\left\{\cot(\varphi)(M_{11}-M_{22})+M_{11,\varphi}+\frac{1}{\sin(\varphi)}M_{12,\theta}-RQ_1\right\}=I_2\ddot{u}_1^0+I_3\ddot{\psi}_1$$

$$\delta\psi_2 \quad : \quad \frac{1}{R}\left\{2\cot(\varphi)M_{12}+M_{12,\varphi}+\frac{1}{\sin(\varphi)}M_{22,\theta}-RQ_2\right\}=I_2\ddot{u}_2^0+I_3\ddot{\psi}_2 \tag{18}$$

The governing equations of motion in terms of the displacements field for the FG-GPLRC spherical sell may be obtained using Eqs. (13)-(18). The resulting equations are

$$\frac{1}{R^2}\{\cot(\varphi)\Big[A_{11}u_{1,\varphi}^0-\frac{A_{11}+A_{66}}{\sin(\varphi)}u_{2,\theta}^0+(A_{12}-A_{11})\cot(\varphi)u_1^0+B_{11}\psi_{1,\varphi}-\frac{B_{11}+B_{66}}{\sin(\varphi)}\psi_{2,\theta}+(B_{12}-B_{11})\cot(\varphi)\psi_1\Big]+A_{11}u_{1,\varphi\varphi}^0+\frac{1}{\sin^2(\varphi)}\big[A_{66}u_{1,\theta\theta}^0-A_{12}u_1^0\big]+B_{11}\psi_{1,\varphi\varphi}+\frac{1}{\sin^2(\varphi)}\big[B_{66}\psi_{1,\theta\theta}-B_{12}\psi_1\big]+\frac{A_{12}+A_{66}}{\sin(\varphi)}u_{2,\varphi\theta}^0+\frac{B_{12}+B_{66}}{\sin(\varphi)}\psi_{2,\varphi\theta}+(A_{11}+A_{12})u_{3,\varphi}^0+A_{55}\big[u_{3,\varphi}^0-u_1^0+R\psi_1\big]\}=I_1\ddot{u}_1^0+I_2\ddot{\psi}_1 \tag{19}$$

$$\frac{1}{R^2}\{\cot(\varphi)\Big[A_{66}u_{2,\varphi}^0+\frac{A_{11}+A_{66}}{\sin(\varphi)}u_{1,\theta}^0-2A_{66}\cot(\varphi)u_2^0+B_{66}\psi_{2,\varphi}+\frac{B_{11}+B_{66}}{\sin(\varphi)}\psi_{1,\theta}-2B_{66}\cot(\varphi)\psi_2\Big]+A_{66}u_{2,\varphi\varphi}^0+\frac{1}{\sin^2(\varphi)}\big[A_{11}u_{2,\theta\theta}^0+A_{66}u_2^0\big]+B_{66}\psi_{2,\varphi\varphi}+\frac{1}{\sin^2(\varphi)}\big[B_{11}\psi_{2,\theta\theta}+B_{66}\psi_2\big]+\frac{A_{12}+A_{66}}{\sin(\varphi)}u_{1,\varphi\theta}^0+\frac{B_{12}+B_{66}}{\sin(\varphi)}\psi_{1,\varphi\theta}+\frac{(A_{11}+A_{12})}{\sin(\varphi)}u_{3,\theta}^0+A_{44}\Big[\frac{1}{\sin(\varphi)}u_{3,\theta}^0-u_2^0+R\psi_2\Big]\}=I_1\ddot{u}_2^0+I_2\ddot{\psi}_2 \tag{20}$$

$$\frac{1}{R^2}\{\cot(\varphi)\Big[B_{11}u_{1,\varphi}^0-\frac{B_{11}+B_{66}}{\sin(\varphi)}u_{2,\theta}^0+(B_{12}-B_{11})\cot(\varphi)u_1^0+D_{11}\psi_{1,\varphi}-\frac{D_{11}+D_{66}}{\sin(\varphi)}\psi_{2,\theta}+(D_{12}-D_{11})\cot(\varphi)\psi_1\Big]+B_{11}u_{1,\varphi\varphi}^0+\frac{1}{\sin^2(\varphi)}\big[B_{66}u_{1,\theta\theta}^0-B_{12}u_1^0\big]+D_{11}\psi_{1,\varphi\varphi}+\frac{1}{\sin^2(\varphi)}\big[D_{66}\psi_{1,\theta\theta}-D_{12}\psi_1\big]+\frac{B_{12}+B_{66}}{\sin(\varphi)}u_{2,\varphi\theta}^0+\frac{D_{12}+D_{66}}{\sin(\varphi)}\psi_{2,\varphi\theta}+(B_{11}+B_{12})u_{3,\varphi}^0-RA_{55}\big[u_{3,\varphi}^0-u_1^0+R\psi_1\big]\}=I_2\ddot{u}_1^0+I_3\ddot{\psi}_1 \tag{22}$$

$$\frac{1}{R^2}\{\cot(\varphi)\Big[B_{66}u_{2,\varphi}^0+\frac{B_{11}+B_{66}}{\sin(\varphi)}u_{1,\theta}^0-2B_{66}\cot(\varphi)u_2^0+D_{66}\psi_{2,\varphi}+\frac{D_{11}+D_{66}}{\sin(\varphi)}\psi_{1,\theta}-2D_{66}\cot(\varphi)\psi_2\Big]+B_{66}u_{2,\varphi\varphi}^0+\frac{1}{\sin^2(\varphi)}\big[B_{11}u_{2,\theta\theta}^0+B_{66}u_2^0\big]+D_{66}\psi_{2,\varphi\varphi}+\frac{1}{\sin^2(\varphi)}\big[D_{11}\psi_{2,\theta\theta}+D_{66}\psi_2\big]+\frac{B_{12}+B_{66}}{\sin(\varphi)}u_{1,\varphi\theta}^0+\frac{D_{12}+D_{66}}{\sin(\varphi)}\psi_{1,\varphi\theta}+\frac{(B_{11}+B_{12})}{\sin(\varphi)}u_{3,\theta}^0-RA_{44}\Big[\frac{1}{\sin(\varphi)}u_{3,\theta}^0-u_2^0+R\psi_2\Big]\}=I_2\ddot{u}_2^0+I_3\ddot{\psi}_2 \tag{23}$$

in which I_1, I_2, and I_3 are the inertia terms which defined by

$$(I_1,I_2,I_3)=\sum_{k=1}^{N_L}\int_{z_k}^{z_{k+1}}\rho^{(k)}\left(1+\frac{z}{R}\right)^2(1,z,z^2)dz \tag{24}$$

moreover, In the motion equations, A_{ij} , B_{ij} and D_{ij} coefficients denote the stretching, bending-stretching, and bending stiffness in the composite media. After combining several layers of graphene, the GPLs are created, assuming uniform distribution and random orientation, each layer of the nanocomposite is homogeneous and isotropic, but after layering due to changing the mass fraction of GPL from one layer to another whole the structure is heterogeneous. Now if the mass fraction of the layers are symmetric to the middle surface, like X, O, and U model of functionally graded the shell will be isotropic and the stretching-bending coupling stiffness matrix Bij will be zero, otherwise this matrix will have a nonzero value.

$$\left(A_{ij},B_{ij},D_{ij}\right)=\sum_{k=1}^{N_L}\int_{z_k}^{z_{k+1}}\left(Q_{ij}^{(k)},zQ_{ij}^{(k)},z^2Q_{ij}^{(k)}\right)dz, \tag{25}$$

$$i,j=1,2,4,5,6$$

The governing equations are accompanied by the boundary conditions. the following, three kinds of boundary conditions that was used extensively are considered, namely the clamped edge boundary conditions (C), the simply supported edge boundary conditions (S) and the free edge boundary conditions (F). Equations describing the boundary conditions on the circumferential edges ($\varphi = \varphi_{in}$ and $\varphi = \varphi_{out}$) can be written as

$$\text{for simply supported edges (S)}: u_1^0 = u_2^0 = u_3^0 = M_{11} = \psi_2 = 0$$

$$\text{for clamped edges (C)}: u_1^0 = u_2^0 = u_3^0 = \psi_1 = \psi_2 = 0$$

$$\text{for free edges (F)}: N_{11} = N_{12} = Q_1 = M_{11} = M_{12} = 0, \tag{26}$$

Since that shell is assumed close in the circumferential direction, the kinematical and physical compatibility should be satisfied at the common meridian with ($\theta = 0{,}2\pi$). The kinematical compatibility conditions consists the continuity of displacement components; Also, The physical compatibility conditions can only be the five continuous conditions for the stress resultants and related equations are

Kinematical compatibility conditions

$$\begin{gathered} u_1^0(\varphi,0,t) = u_1^0(\varphi,2\pi,t), \\ u_2^0(\varphi,0,t) = u_2^0(\varphi,2\pi,t), \\ u_3^0(\varphi,0,t) = u_3^0(\varphi,2\pi,t), \\ \psi_1(\varphi,0,t) = \psi_1(\varphi,2\pi,t), \\ \psi_2(\varphi,0,t) = \psi_2(\varphi,2\pi,t); \end{gathered} \tag{27}$$

Physical compatibility conditions

$$\begin{gathered} N_{12}(\varphi,0,t) = N_{12}(\varphi,2\pi,t), \\ N_{22}(\varphi,0,t) = N_{22}(\varphi,2\pi,t), \\ Q_2(\varphi,0,t) = Q_2(\varphi,2\pi,t), \\ M_{12}(\varphi,0,t) = M_{12}(\varphi,2\pi,t), \\ M_{22}(\varphi,0,t) = M_{22}(\varphi,2\pi,t); \end{gathered} \tag{28}$$

4. GDQ method

The GDQ method will be used to discretize the derivatives in the derived motion equations and the associated boundary conditions. This method permits to approximate the first, second and higher order derivative in an arbitrary point in the 2-D spherical shell domain (φ_p, θ_q) of a smooth function $\mathbf{u}$ using a weighted linear sum of the function values at some defined distributed points. For example implementing GDQ technique to the first and second order derivatives given as follow (Artioli and Viola 2005, Tornabene and Viola 2007, Javani *et al.* 2019)

$$\begin{gathered} \mathbf{u}_{,\varphi}|_{\varphi=\varphi_p,\theta=\theta_q} = \sum_{p'=1}^{N_\varphi}\sum_{q'=1}^{N_\theta} C_{pp'}^{\varphi}\delta_{qq'}^{\theta}\mathbf{u}|_{\varphi=\varphi_{p'},\theta=\theta_{q'}} \\ \mathbf{u}_{,\theta}|_{\varphi=\varphi_p,\theta=\theta_q} = \sum_{p'=1}^{N_\varphi}\sum_{q'=1}^{N_\theta} \delta_{pp'}^{\varphi}C_{qq'}^{\theta}\mathbf{u}|_{\varphi=\varphi_{p'},\theta=\theta_{q'}} \\ \mathbf{u}_{,\theta\theta}|_{\varphi=\varphi_p,\theta=\theta_q} = \sum_{p'=1}^{N_\varphi}\sum_{q'=1}^{N_\theta} \delta_{pp'}^{\varphi}\bar{C}_{qq'}^{\theta}\mathbf{u}|_{\varphi=\varphi_{p'},\theta=\theta_{q'}}, \\ p = 1,2,\ldots,N_\varphi, \qquad q = 1,2,\ldots,N_\theta \end{gathered} \tag{29}$$

where N_φ and N_θ are the number of grid points in the φ and θ-directions, respectively. $\delta_{pp'}^{\varphi}$ and $\delta_{qq'}^{\theta}$ are equal to one when $p = p'$ and $q = q'$. Also, $C_{pp'}^{\varphi}$ and Cqq'^{θ} associated $\bar{C}_{pp'}^{\varphi}$ and $\bar{C}_{qq'}^{\theta}$ are the weighting coefficients of the first and second order derivatives, respectively, and are determined by means of the Lagrange interpolated polynomials, which can be defined by the following formula

$$\begin{gathered} C_{pp'}^{\varphi} = \begin{cases} \dfrac{\Pi(\varphi_p)}{(\varphi_p - \varphi_{p'})\Pi(\varphi_{p'})} & when \quad p \neq p' \\ -\displaystyle\sum_{k=1,k\neq p}^{N_\varphi} C_{pk}^{\varphi} & when \quad p = p' \end{cases} \\ C_{qq'}^{\theta} = \begin{cases} \dfrac{\Pi(\theta_q)}{(\theta_q - \theta_{q'})\Pi(\theta_{q'})} & when \quad q \neq q' \\ -\displaystyle\sum_{k=1,k\neq q}^{N_\theta} C_{qk}^{\theta} & when \quad q = q' \end{cases} \\ p,p' = 1,2,\ldots,N_\varphi \qquad q,q' = 1,2,\ldots,N_\theta \end{gathered} \tag{30}$$

in which

$$\begin{gathered} \Pi(\varphi_p) = \prod_{k=1,k\neq p}^{N_\varphi} (\varphi_p - \varphi_k), \\ \Pi(\theta_q) = \prod_{k=1,k\neq q}^{N_\theta} (\theta_q - \theta_k) \end{gathered} \tag{31}$$

and

$$\begin{gathered} \begin{cases} \bar{C}_{pp'}^{\varphi} = 2\left(C_{pp}^{\varphi}C_{pp'}^{\varphi} - \dfrac{C_{pp'}^{\varphi}}{(\varphi_p - \varphi_{p'})}\right), & p \neq p' \\ p,p' = 1,2,\ldots,N_\varphi \end{cases} \\ \begin{cases} \bar{C}_{pp}^{\varphi} = -\displaystyle\sum_{k=1,k\neq p}^{N_\varphi} \bar{C}_{pk}^{\varphi}, & p = p', \\ p = 1,2,\ldots,N_\varphi \end{cases} \\ \begin{cases} \bar{C}_{qq'}^{\theta} = 2\left(C_{qq}^{\theta}C_{qq'}^{\theta} - \dfrac{C_{qq'}^{\theta}}{(\theta_q - \theta_{q'})}\right), & q \neq q' \\ q,q' = 1,2,\ldots,N_\theta \end{cases} \\ \begin{cases} \bar{C}_{qq}^{\theta} = -\displaystyle\sum_{k=1,k\neq q}^{N_\theta} \bar{C}_{qk}^{\theta}, & q = q' \\ q = 1,2,\ldots,N_\theta \end{cases} \end{gathered} \tag{32}$$

The accuracy of this method is usually sensitive to the grid point distribution. The nodes must be located across the domain according to a specific grid distribution. In the present research, the Chebyshev-Gauss-Lobatto grid distribution is used due to its stability and accuracy. In this type of dispensation, the discrete points in the φ and θ-directions are defined as

$$\begin{gathered} \varphi_p = (\varphi_{out} - \varphi_{in})\left(\frac{1}{2} - \frac{1}{2}\cos\left(\frac{p-1}{N_\varphi - 1}\pi\right)\right) + \varphi_{in}, \\ p = 1,2,\ldots,N_\varphi \end{gathered} \tag{33}$$

Table 2 Convergence of first three natural frequencies results for a FS functionally graded multilayer X-GPLRC spherical shell ($h/R = 0.05$, $\varphi_{in} = 15°$, $\varphi_{out} = 90°$, $W_{GPL} = 0.3\%$, and $\nu = 0.3$)

			N_L					
mode	N_θ	N_φ	4	6	8	10	12	14
Ω_1	15	15	14.2932	14.3829	14.4136	14.4277	14.4354	14.4400
		17	14.2909	14.3805	14.4112	14.4253	14.4329	14.4375
		19	14.2905	14.3800	14.4107	14.4249	14.4325	14.4371
	17	15	14.2928	14.3824	14.4131	14.4272	14.4349	14.4395
		17	14.2904	14.3800	14.4107	14.4248	14.4324	14.4370
		19	14.2900	14.3796	14.4103	14.4244	14.4320	14.4366
	19	15	14.2928	14.3824	14.4132	14.4273	14.4349	14.4395
		17	14.2904	14.3800	14.4107	14.4248	14.4325	14.4371
		19	14.2901	14.3796	14.4103	14.4244	14.4320	14.4366
Ω_2	15	15	15.4710	15.4751	15.4765	15.4771	15.4775	15.4777
		17	15.4711	15.4751	15.4765	15.4772	15.4775	15.4777
		19	15.4711	15.4751	15.4765	15.4772	15.4775	15.4777
	17	15	15.4710	15.4751	15.4765	15.4771	15.4775	15.4777
		17	15.4711	15.4751	15.4765	15.4772	15.4775	15.4777
		19	15.4711	15.4751	15.4765	15.4772	15.4775	15.4777
	19	15	15.4710	15.4751	15.4765	15.4771	15.4775	15.4777
		17	15.4711	15.4751	15.4765	15.4772	15.4775	15.4777
		19	15.4711	15.4751	15.4765	15.4772	15.4775	15.4777
Ω_3	15	15	21.0336	21.0479	21.0529	21.0552	21.0564	21.0572
		17	21.0335	21.0479	21.0529	21.0552	21.0564	21.0572
		19	21.0335	21.0479	21.0529	21.0552	21.0564	21.0572
	17	15	21.0336	21.0479	21.0529	21.0552	21.0564	21.0572
		17	21.0335	21.0479	21.0529	21.0552	21.0564	21.0572
		19	21.0335	21.0479	21.0529	21.0552	21.0564	21.0572
	19	15	21.0336	21.0479	21.0529	21.0552	21.0564	21.0572
		17	21.0335	21.0479	21.0529	21.0552	21.0564	21.0572
		19	21.0335	21.0479	21.0529	21.0552	21.0564	21.0572

$$\theta_q = 2\pi\left(\frac{1}{2} - \frac{1}{2}\cos\left(\frac{q-1}{N_\theta - 1}\pi\right)\right), \quad q = 1,2,\ldots,N_\theta \tag{34}$$

The discretized equations of motion and boundary conditions after applying GDQ method are not given here for the sake of brevity; meanwhile, one may refer to the other available works, e.g., (Tornabene and Viola 2007). Obtained algebraic eigenvalue problem may be written in compact form as follows

$$\mathbf{M}]\{\ddot{u}\} + [\mathbf{K}]\{u\} = 0 \tag{35}$$

where $\{u\}$ is the displacement vector with $(5 \times N_\varphi \times N_\theta)$ components and including unknown displacements field $(u^0_{1pq}, u^0_{2pq}, u^0_{3pp}, \psi_{1pq}, \psi_{2pq})$. Furthermore, in the above equation, $[\mathbf{M}]$ is the mass matrix and $[\mathbf{K}]$ is the stiffness matrix. Since the free vibration of the FG-GPLRC spherical shell on elastic foundation is harmonic, one can assume the following periodic form for the displacement functions

Table 1 mechanical properties of the matrix and GPLs (Wu 2017)

Properties	Epoxy	GPL
Elasticity modulus(E)[GPa]	3.0	1010
Mass density (ρ) [kg/m ^{3}]	1200	1062.5
Poisson's ratio (ν)	0.34	0.186

$$\begin{aligned} u^0_1(\varphi,\theta,t) &= U^0_1(\varphi,\theta)\sin(\omega t + \alpha) \\ u^0_2(\varphi,\theta,t) &= U^0_2(\varphi,\theta)\sin(\omega t + \alpha) \\ u^0_3(\varphi,\theta,t) &= U^0_3(\varphi,\theta)\sin(\omega t + \alpha) \\ \psi_1(\varphi,\theta,t) &= \Psi_1(\varphi,\theta)\sin(\omega t + \alpha) \\ \psi_2(\varphi,\theta,t) &= \Psi_2(\varphi,\theta)\sin(\omega t + \alpha) \end{aligned} \tag{36}$$

Substituting Eq. (36) into Eq.(35), the following algebraic eigenvalue equations in the matrix form which yield the natural frequencies and the corresponding mode

Table 3 Comparison of the frequency parameters $\Omega = \omega R\sqrt{\rho(1-\nu^2)/E}$ for an isotropic FS hemispherical shell ($\varphi_{in} = 0$, $\varphi_{out} = 90°$ and $R = 1$ m)

modes		$h/R = 0.01$			$h/R = 0.05$		
n	m	Present	Artioli and Viola (2006)	Qu *et al.* (2013)	Present	Artioli and Viola (2006)	Qu *et al.* (2013)
0	1	0.7138	0.7138	0.7138	0.7362	0.7364	0.7360
	2	0.8891	0.8892	0.8891	0.9587	0.9605	0.9583
	3	0.9337	0.9338	0.9336	1.1694	1.1744	1.1690
	4	0.9664	0.9667	0.9663	1.1826	1.1832	1.1832
	5	1.0097	1.0102	1.0097	1.4785	1.4859	1.4780
1	1	0.5343	0.5343	0.5343	0.5422	0.5421	0.5422
	2	0.8445	0.8444	0.8444	0.8788	0.8796	0.8785
	3	0.9162	0.9163	0.9162	1.0535	1.0573	1.0535
	4	0.9498	0.9501	0.9498	1.3218	1.3300	1.3213
	5	0.9863	0.9867	0.9862	1.6461	1.6511	1.6463
2	1	0.8589	0.8589	0.8589	0.8767	0.8763	0.8764
	2	0.9217	0.9215	0.9217	0.9970	0.9946	0.9966
	3	0.9510	0.9507	0.9510	1.1917	1.1869	1.1913
	4	0.9781	0.9773	0.9781	1.5238	1.5191	1.5232
	5	1.0169	1.0155	1.0169	1.9788	1.9789	1.9782

shapes of the spherical shell are obtained

$$(\mathbf{K} - \boldsymbol{\omega}^2\mathbf{M})\mathbf{U} = 0 \tag{37}$$

in which $\boldsymbol{\omega}$ and $\mathbf{U}$ are the natural frequency and the corresponding mode shape obtained by solving the above eigenvalue equation.

5. Results and discussion

The developed process in the previous section is implemented in the rest to analyse the free vibration characteristics of FG-GPLRC Spherical shell resting on a two parameter elastic foundation. Unless otherwise mentioned, a nanocomposite consisted an epoxy matrix embedded by graphene platelets. The mechanical properties for these constituents are given in Table 1.

Different boundary conditions with the combination of clamped (C), simply-supported (S), and free (F) are considered at the circumferential edges of structure. For instance, the FC boundary condition indicates which shell is Free at $\varphi = \varphi_{in}$ and which one is clamped at $\varphi = \varphi_{out}$. In the present research, to investigate the effects of elastic coefficients on natural frequencies of the shell, the nondimensional Winkler and Pasternak coefficients are appointed according to

$$K_w = \frac{k_w R^4(1-\nu_m^2)}{E_m h^3}$$
$$K_g = \frac{k_g R^2(1-\nu_m^2)}{E_m h^3} \tag{38}$$

Furthermore, the nondimensional natural frequencies of mentioned structure are defined as

$$\Omega_i = \omega_i R^2\sqrt{\frac{\rho_m(1-\nu_m^2)}{E_m h^2}} \tag{39}$$

All of the numerical results are obtained considering the following dimensions of reinforcement

$$a_{GPL} = 2.5\mu\text{m},\ b_{GPL} = 1.5\mu\text{m},\ t_{GPL} = 1.5\text{nm}.$$

5.1 Convergence and comparison study

A convergence study is performed to obtain the optimum number of layers. The aim beyond this study is to obtain the number of required grid points in the meridional and circumferential directions to reach the converged natural frequencies Ω. The results of the converged first three nondimensional natural frequency of the FG-GPLRC spherical shell with $h/R = 0.05$ are presented in Table 2. Moreover, the weight fraction of fillers is selected as $W_{GPL} = 0.3\%$ and X-GPLRC pattern is considered. At the $\varphi_{in} = 15°$ free edge and at the $\varphi_{out} = 90°$ simply-supported are assumed (FS). As seen from the results of related figure, after assumption of 19 grid point across the shell domain, the results are converged. Therefore, to obtain high accurate results for the subsequent results, the number of grid points is set equal to $N_\varphi = N_\theta = 21$. Another result of this study states that there is a very small difference between the natural frequencies at $N_L = 10$ and $N_L > 10$ therefore a multilayer GPLRC shell with 10 layers could offer sufficient accuracy to model the ideal functionally graded shell with smooth variations between material compositions and properties. In the rest of the paper, all of results of the FG-GPLRC shell will be obtained with 10 layers.

Table 4 Comparison of natural frequency parameter $\lambda = \omega h\sqrt{\rho_m/E_m}$ for a FG-GPLRC annular plate with weight fraction of reinforcements $W_{GPL} = 1\%$

		B.Cs.		
Graded type	Source	CC	CS	CF
U-GPLRC	Present	0.2207	0.1526	0.0344
	Malekzadeh *et al*. (2018)	0.22095	0.15274	0.03445
X-GPLRC	Present	0.2485	0.1740	0.0398
	Malekzadeh *et al*. (2018)	0.24454	0.17090	0.03899
O-GPLRC	Present	0.1829	0.1246	0.0277
	Malekzadeh *et al*. (2018)	0.19038	0.13001	0.02898
Λ-GPLRC	Present	0.2024	0.1418	0.0311
	Malekzadeh *et al*. (2018)	0.20598	0.14149	0.03174

Since there is no the free vibration study on the FG-GPLRC spherical shell in the open access literature, the comparison of frequency characteristics for isotropic shell with FS boundary condition are provided in Table 3. In this comparative study, frequency parameter is defined $\Omega = \omega R\sqrt{\rho(1-\nu^2)/E}$ for the hemispherical shells with geometrical parameters $\varphi_{in} = 0$, $\varphi_{out} = 90°$, $R = 1$ m, and $h/R = 0.01$ and 0.05. In this study n denotes circumferential modes and m indicates meridional modes.

The results are compared with other works by Artioli and Viola (2006) using the GDQ method and Qu *et al.* (2013) using the variational method. An excellent agreement is seen for each thickness-to-radius ratio.

As mentioned in the introduction section, there is no related research on the free vibration of nanocomposite spherical shells reinforced with graphene platelets. However for the case of annular plates, results of Malekzadeh *et al.* (2018) could be mentioned. The spherical shell can be reduce to an annular plate considering zero rise in the shell. In order to compare, the radius of curvature is set equal to a large number, i.e., $R = 10^5$m and opening angles must be must be corresponding to radius, for this condition, $\varphi_{in} = 0.25 \times 10^{-5}$ rad and $\varphi_{out} = 10^{-5}$ rad. The thickness is set equal to $h = 0.1$ m. Under such conditions, the inner and outer radius of the annular plate will be $R\varphi_{in} = 0.25$ m and $R\varphi_{out} = 1$ m, respectively, which is the same as the one provided by Malekzadeh et al. (2018). Comparison of fundamental frequency parameter $\lambda = \omega h\sqrt{\rho_m/E_m}$ for three types of boundary conditions (CC, CS, CF) and four functionally graded patterns of fillers distribution along thickness are provided in Table 4. It can be seen that results are in good agreement with those of Malekzadeh *et al*. (2018) which are obtained by means of the transformed differential quadrature method.

5.2 Parametric study

After validating the present formulation and proposed method, novel numerical results are given in this section. It is worth noting that repeated frequencies were not considered in this research.

Variations of the first five nondimensional natural frequencies of the FG-GPLRC spherical shell are provided in Table 5 for three values of weight fractions and four types of GPLs distributions. Annular spherical shell with thickness ratio $h/R = 0.05$ and opening angles $\varphi_{in} = 15°$ and $\varphi_{out} = 90°$ are assumed. Also, the effects of various boundary conditions are taken into account. It is evident that the higher values of nanofillers weight fractions will increase of the nondimensional natural frequency. Furthermore, the shell with functionally graded X-GPLRC and O-GPLRC types of distribution showed the highest and lowest natural frequencies, respectively. Also, shells with clamped edges and free edges exhibited the highest and least increasing impact on nondimensional natural frequency.

Variations of the nondimensional frequencies of clamped (CC) FG-GPLRC spherical shell for different values of φ_{in} and φ_{out} are listed in Table 6. This figure is associated to elastic foundation with $(K_w, K_g) = (0,0), (200,0), (0,20)$ and $(200,20)$, respectively. For developing the numerical results of this figure, $h/R = 0.05$ and $W_{GPL} = 0.3\%$ are assumed. It is clear that for the φ_{in} values, the increases in φ_{out} of shell results in decline of the natural frequency of X patterns of FG-GPLRC structure, while for the same values of φ_{out}, the increment of angle φ_{in} the natural frequencies tended to a higher values. Therefore, one can state that the increase in the length of the clamped spherical shell in the meridional direction will augment the shell flexiblity and reduce the non-dimensional frequency. On the other hand, increase of the nondimensional
Winkler and Pasternak coefficients results in higher natural frequencies.

For different combinations of boundary conditions, the nondimensional fundamental frequency of X, O and U patterns of FG-GPLRC multilayer spherical shell is evaluated as presented in Table 7. For developing the results of this figure, $\varphi_{in} = 15°$, $\varphi_{out} = 120°$, $W_{GPL} = 0.3\%$ and $(K_w, K_g) = (100,10)$ are assumed. For this example various thickness-to-radius ratio are taken into consideration which are $h/R = 0.01, 0.05, 0.1$. It can be concluded that boundary conditions play a key role in the vibrational behavior of the shell and considerably effects the natural frequencies. For less flexible boundary conditions, the spherical shell is more stable and caused

Table 5 The influences of GPL distribution pattern, weight fraction and boundary conditions on the first five dimensionless frequency parameter Ω of FG-GPLRC spherical shells ($h/R = 0.05$, $\varphi_{in} = 15°$, $\varphi_{out} = 90°$ and $(K_w, K_g) = (0,0)$)

			mode				
B.Cs.	W_{GPL}(%)	Graded type	Ω_1	Ω_2	Ω_3	Ω_4	Ω_5
CC	0.1	U-GPLRC	20.537	21.393	21.473	22.089	23.510
		X-GPLRC	20.796	21.545	21.624	22.224	23.633
		O-GPLRC	20.270	21.148	21.397	21.952	23.270
		Λ-GPLRC	20.441	21.308	21.416	22.009	23.426
	0.3	U-GPLRC	25.145	26.192	26.290	27.045	28.784
		X-GPLRC	25.771	26.465	26.743	27.372	29.081
		O-GPLRC	24.479	25.577	26.099	26.704	28.153
		Λ-GPLRC	24.798	25.882	26.119	26.791	28.429
	0.5	U-GPLRC	29.032	30.242	30.355	31.226	33.234
		X-GPLRC	29.931	30.606	31.025	31.698	33.661
		O-GPLRC	28.063	29.343	30.075	30.731	32.307
		Λ-GPLRC	28.450	29.716	30.083	30.817	32.628
CS	0.1	U-GPLRC	19.387	20.383	21.385	22.012	23.246
		X-GPLRC	19.570	20.545	21.435	22.121	23.367
		O-GPLRC	19.200	20.214	21.331	21.899	23.107
		Λ-GPLRC	19.210	20.266	21.356	21.961	23.146
	0.3	U-GPLRC	23.737	24.956	26.183	26.950	28.461
		X-GPLRC	24.181	25.346	26.301	27.212	28.744
		O-GPLRC	23.272	24.536	26.044	26.666	28.022
		Λ-GPLRC	23.217	24.594	26.081	26.764	28.150
	0.5	U-GPLRC	27.408	28.815	30.231	31.117	32.861
		X-GPLRC	28.045	29.374	30.400	31.491	33.261
		O-GPLRC	26.731	28.203	30.026	30.700	32.184
		Λ-GPLRC	26.593	28.235	30.059	30.802	32.358
CF	0.1	U-GPLRC	1.403	1.955	3.461	5.972	6.304
		X-GPLRC	1.476	1.990	3.643	5.972	6.626
		O-GPLRC	1.325	1.917	3.266	5.958	5.972
		Λ-GPLRC	1.388	1.948	3.422	5.984	6.233
	0.3	U-GPLRC	1.718	2.393	4.237	7.312	7.718
		X-GPLRC	1.891	2.477	4.671	7.313	8.483
		O-GPLRC	1.520	2.296	3.740	6.836	7.312
		Λ-GPLRC	1.648	2.361	4.061	7.342	7.401
	0.5	U-GPLRC	1.983	2.764	4.893	8.444	8.912
		X-GPLRC	2.231	2.882	5.510	8.445	10.002
		O-GPLRC	1.692	2.620	4.158	7.609	7.610
		Λ-GPLRC	1.859	2.705	4.576	8.345	8.488

higher nondimensional natural frequencies. On the other hand, it can be inferred that for different boundary conditions, by increase of the shell thickness ratio, the frequencies of the structure increase while influences of functionally graded patterns showed a decline.

Fig. 2 aims to analyse the effect of the spherical shell opening angle (φ_{out}) in different boundary conditions. In this example, shells with CC, SS, CS, and FS types of boundary conditions are considered. Four different amounts of elastic foundation coefficients for X-GPLRC spherical shells with geometrical characteristics $h/R = 0.05$ and $\varphi_{in} = 30°$ is taken as case studies. Also, weight fraction of graphene platelets is set to $W_{GPL} = 0.3\%$. It is again verified that, the higher natural frequency belongs to higher Winkler and Pasternak elastic coefficients.

Table 6 The influences of opening angles and elastic foundation coefficients on the first five dimensionless frequency parameter Ω of clamped X-GPLRC spherical shells ($h/R = 0.05$ and $W_{GPL} = 0.3\%$)

			mode				
(K_w, K_g)	φ_{in}	φ_{out}	Ω_1	Ω_2	Ω_3	Ω_4	Ω_5
(0,0)	10	60	31.945	34.039	35.320	38.895	39.220
		90	24.426	25.006	25.536	27.113	27.999
		120	17.597	17.971	20.486	22.433	22.954
	20	60	37.860	38.051	41.203	41.361	44.873
		90	27.422	27.562	27.853	28.518	29.608
		120	19.384	20.791	22.888	23.424	23.757
	30	60	49.141	49.418	51.016	51.475	53.038
		90	29.554	30.284	30.563	32.089	33.026
		120	21.530	23.224	24.714	25.274	25.557
(200,0)	10	60	34.670	36.698	37.707	41.153	41.584
		90	27.243	27.316	28.489	30.239	30.742
		120	19.898	20.461	25.400	25.690	28.035
	20	60	40.235	40.458	43.392	43.612	47.013
		90	30.178	30.381	30.907	30.983	32.602
		120	22.232	22.877	22.888	26.301	26.338
	30	60	51.046	51.308	52.864	53.320	54.871
		90	32.461	32.953	33.474	34.607	35.482
		120	24.380	25.649	26.407	27.499	27.565
(0,20)	10	60	39.058	39.711	44.297	44.983	52.030
		90	27.982	29.304	29.808	33.032	33.407
		120	19.464	20.486	20.498	24.892	25.839
	20	60	45.330	46.826	48.045	50.148	53.857
		90	31.491	32.379	34.062	34.274	36.207
		120	22.726	22.888	22.928	26.001	26.818
	30	60	58.192	59.172	59.551	60.439	63.278
		90	34.568	35.838	36.738	39.123	40.566
		120	25.908	25.930	26.407	27.467	28.591
(200,20)	10	60	41.284	41.785	46.356	47.049	53.801
		90	29.669	31.818	32.097	34.146	35.355
		120	20.486	21.044	22.871	27.487	28.111
	20	60	47.312	48.734	49.962	52.076	55.599
		90	33.917	34.127	36.408	36.567	38.335
		120	22.888	24.278	25.231	28.557	29.030
	30	60	59.795	60.774	61.125	62.055	64.772
		90	36.873	38.244	38.587	41.423	42.523
		120	26.407	27.422	28.182	29.966	30.783

As expected, with the enhancement in φ_{out}, the shell loses its the flexural rigidity; hence the natural frequency declines. Another result states that increase of φ_{out} reduces the influence of elastic foundation coefficients on fundamental natural frequency.

Additionally, changes of nondimensional fundamental frequency of FG-GPLRC spherical shell versus angle φ_{in} with X distribution pattern are depicted in Fig. 3 for different types of boundary conditions and elastic foundation coefficients. In this study shells with $h/R = 0.02$, $W_{GPL} = 0.3\%$ and $\varphi_{out} = 120°$ are examined. The results demonstrate that enhancement of φ_{in}, fundamental frequency is constantly elevate for the shells without free edges while spherical shells with free edges exhibit undetectable behavior.

Table 7 The influences of thickness-to-radius ratio on the fundamental dimensionless frequency parameter Ω_1 of spherical shells with various boundary conditions and types of GPL distribution ($\varphi_{in} = 15°$, $\varphi_{out} = 120°$, $W_{GPL} = 0.3\%$, $(K_w, K_g) = (100{,}10)$)

		B.Cs.							
(h/R)	Graded type	CC	CS	CF	SC	SS	SF	FC	FS
0.01	U-GPLRC	82.340	80.565	8.325	81.070	79.319	7.907	27.912	27.850
	X-GPLRC	82.705	80.817	8.376	81.349	79.490	7.923	29.562	29.499
	O-GPLRC	81.920	80.278	8.267	80.751	79.130	7.889	26.023	25.963
0.05	U-GPLRC	21.250	20.509	5.514	20.648	19.917	5.514	10.393	9.994
	X-GPLRC	21.331	20.643	5.515	20.794	20.006	5.515	10.438	10.006
	O-GPLRC	21.053	20.361	5.515	20.485	19.823	5.515	10.342	9.981
0.1	U-GPLRC	10.749	10.749	2.753	10.749	10.749	2.753	7.085	6.850
	X-GPLRC	10.751	10.751	2.753	10.751	10.751	2.753	7.110	6.856
	O-GPLRC	10.748	10.748	2.753	10.748	10.748	2.753	7.056	6.844

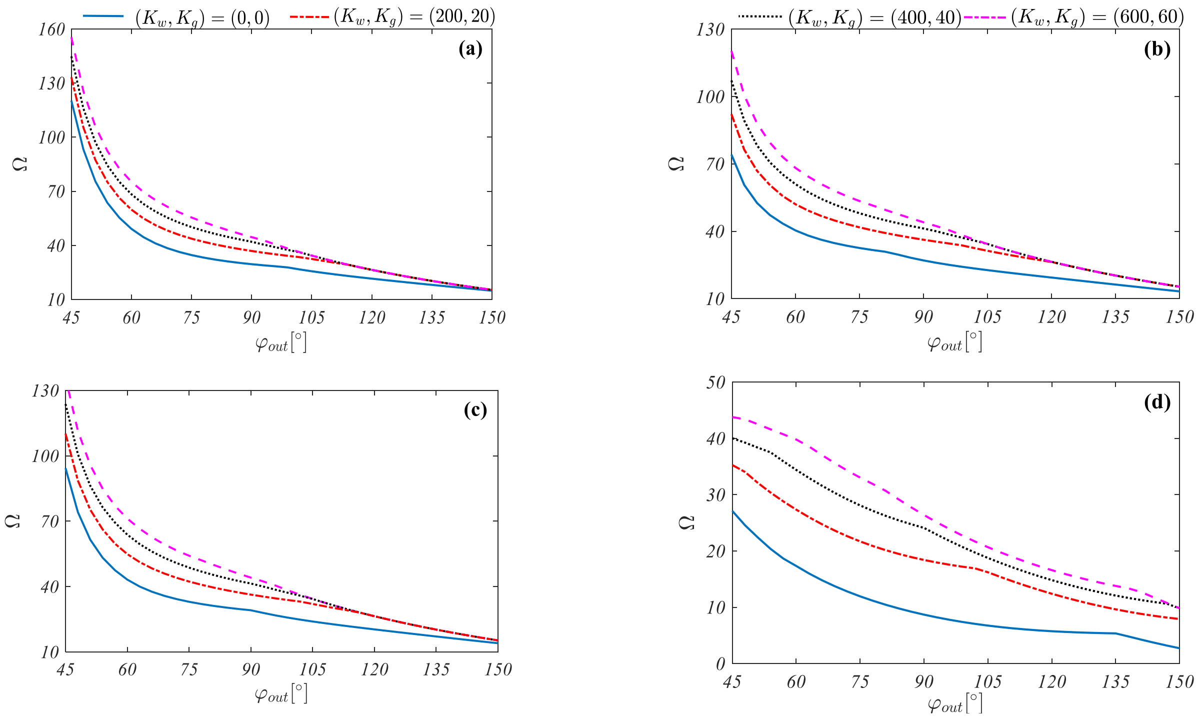

Fig. 2 The variation of the fundamental frequency parameter versus the φ_{out} of the X-GPLRC spherical shells for four elastic coefficients with various boundary conditions ($h/R = 0.05$, $\varphi_{in} = 30°$, $W_{GPL} = 0.3\%$): (a) CC, (b) SS, (c) CS, (d) FS

Fig. 4 demonstrates the effects of the percent of GPLs weight fraction together with various thickness-to-radius ratio on the fundamental frequency parameter of a FC FG-GPLRC spherical shell. This study provides three annular hole at the apex of the X-GPLRC spherical shell $\varphi_{in} = 0°, 20°, 40°$. For developing this example is set to $\varphi_{out} = 90°$. It can be seen that the frequency parameters increase monotonically increased by rise of the GPLs weight fraction for all values of thickness ratio and opening angles. Also, It is observed that the increase of h/R ratio diminishes the nondimensional natural frequency. It is worth noting that the increment in the thickness-to-radius ratio enhanced the structure stability; hence the natural frequency will be increased, but the non-dimensional frequency decreases.

For further clarification of the vibrational behavior of nanocomposite spherical shells reinforced with graphene platelets, the first six mode shapes of a simply-supported (SS) X-GPLRC spherical shell are indicated in Fig. 5. Moreover, the weight fraction $W_{GPL} = 0.5\%$ is regarded for this example. The mentioned shell are assumed with geometrical parameter $h/R = 0.05$, $\varphi_{in} = 15°$, and $\varphi_{out} = 90$.

In the other example, mode shape analysis is provided for various types of boundary conditions and opening

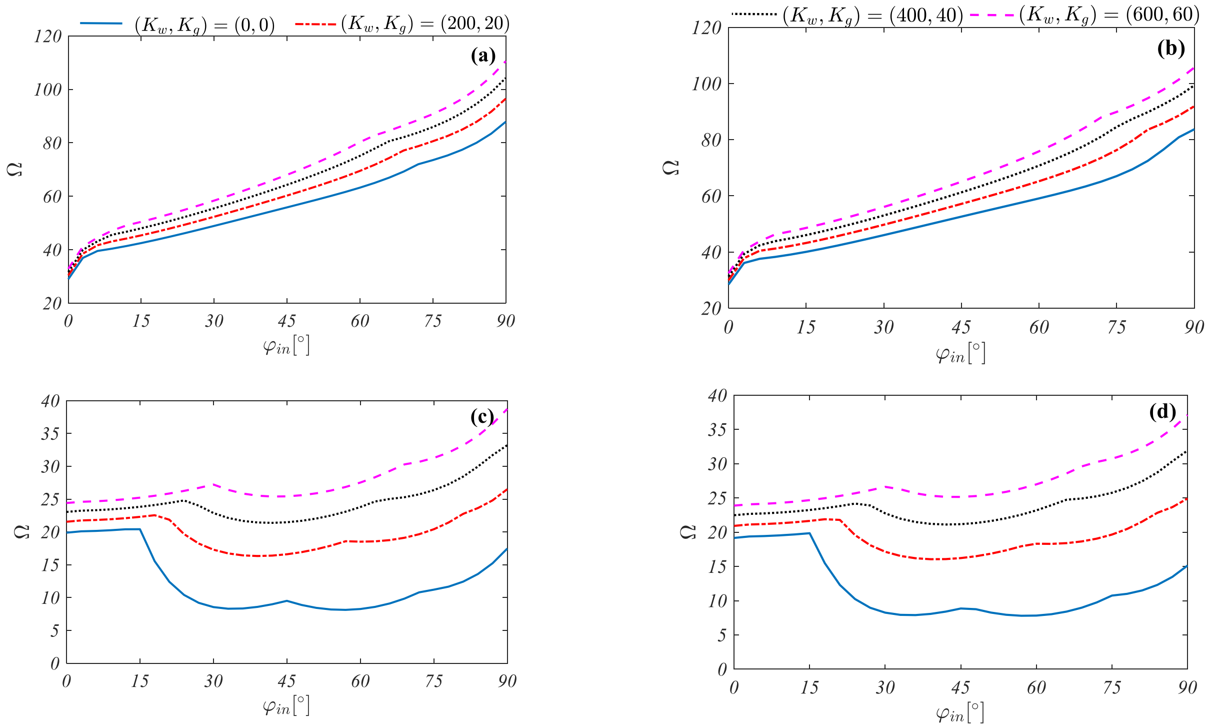

Fig. 3 The variation of the fundamental frequency parameter versus the φ_{in} of the X-GPLRC spherical shells forfour elastic coefficients with various boundary conditions ($h/R = 0.02$, $\varphi_{out} = 120°$, $W_{GPL} = 0.3\%$): (a) CC, (b) SS, (c) FC, (d) FS

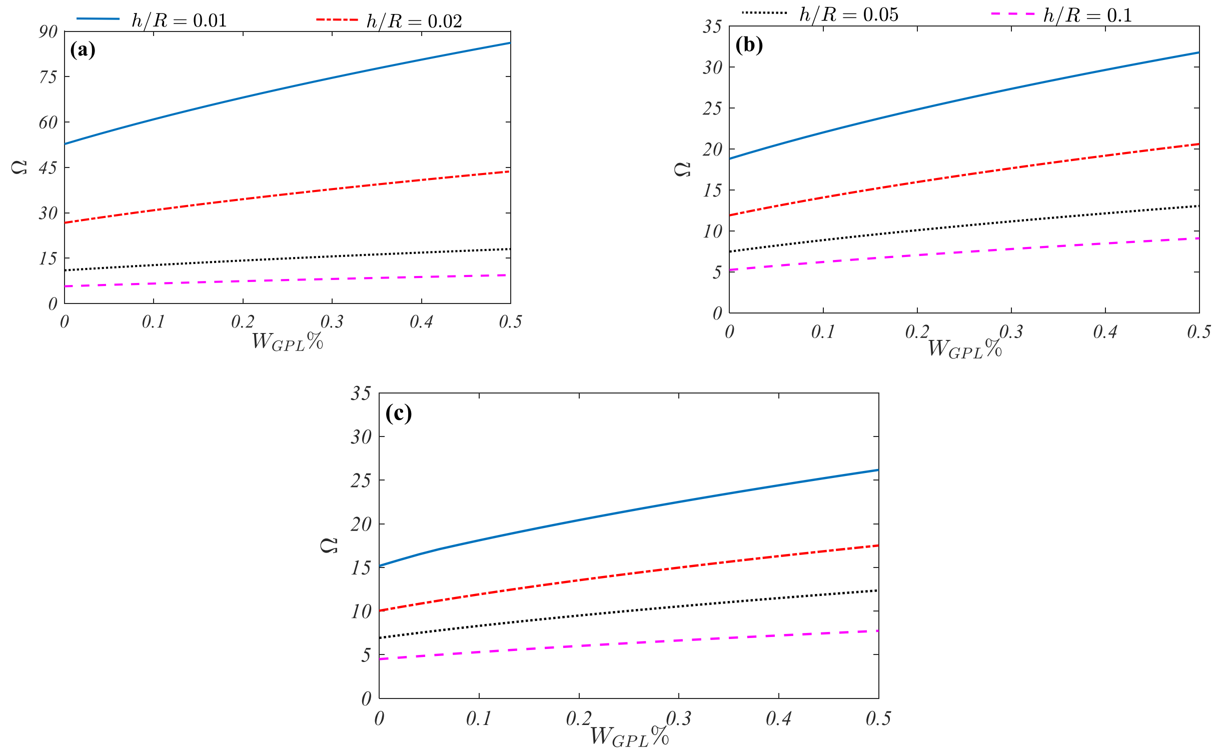

Fig. 4 The variation of the fundamental frequency parameter versus the W_{GPL} of the FC X-GPLRC spherical shells for four thickness ratio with various φ_{in} ($\varphi_{out} = 90°$ and $(K_w, K_g) = (0,0)$): (a) $\varphi_{in} = 0°$, (b) $\varphi_{in} = 20°$, (c) $\varphi_{in} = 40°$

angles in Fig. 6. FG-GPLRC spherical are considered with the weightfraction $W_{GPL} = 0.5\%$ and functionally graded X-type. For developing this study, $\frac{h}{R} = 0.05$ and φ_{in}

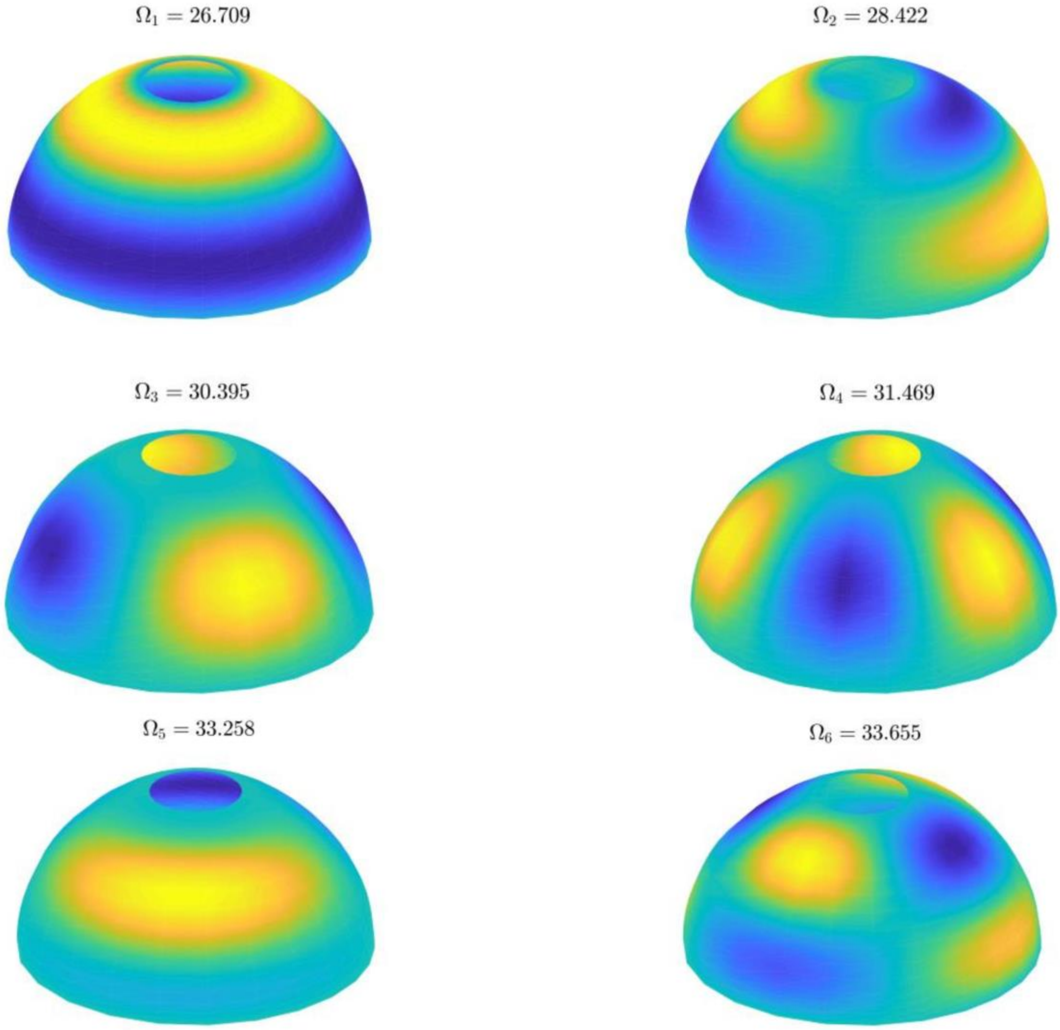

Fig. 5 First six mode shapes of simply-supported X-GPLRC spherical shell ($h/R = 0.05$, $\varphi_{in} = 15°$, $\varphi_{out} = 90°$, $W_{GPL} = 0.5\%$ and $(K_w, K_g) = (0,0)$)

15° are considered. It can be concluded that the boundary conditions and half of opening angle can change the fundamental mode shape of the shell.

6. Conclusions

An analysis is performed in this work to examine the free vibration of the FG-GPLRC spherical shells on the Winkler-Pasternak elastic foundation. The governing motion equations of the shell are established by means of the Sanders kinematic assumptions, first order shell theory and linear elasticity law. These equations are solved by the GDQ method. Following conclusions can be made:

- The weight fractions and functionally graded types of graphene platelets play a significant role in the natural frequencies of FG-GPLRC spherical shell. the non-dimensional frequency of the structure increases by enhancement of weight fraction. Also, the FGX type of GPLs across the thickness direction results in the highest fundamental frequency.
- Variations of φ_{in} and φ_{out} can significantly affect the nondimensional frequency. Generally the longer length spherical shell in φ direction makes the less stable structure hence decreases the non-dimensional natural frequency.
- Types of the boundary conditions play an important role in the vibration characteristics of the spherical shell. The magnitude of natural frequencies for stiffer edge is much higher than the Softer edge. Moreover, the mode shapes exceedingly depend on the types of the boundary conditions of the shell.
- thickness-to-radius ratio of the shell is another important factor in the sphere natural frequency. Results show that as the thickness ratio of the sphere increases, the natural frequencies decreases noticeably.
- Larger elastic foundation coefficients improves the stability of the FG-GPLRC deep spherical shells and so the frequency parameters tend to higher magnitudes.

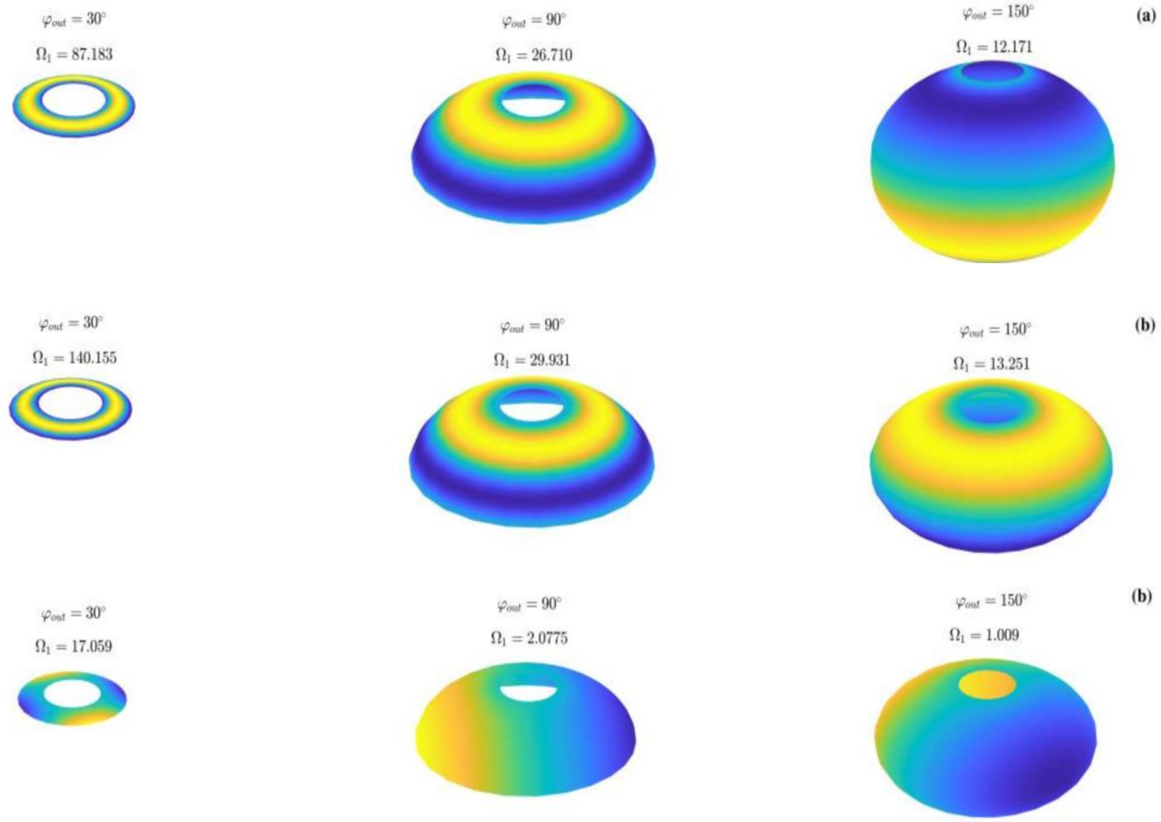

Fig. 6 Effects of boundary conditions and half of opening angle φ_{out} on the fundamental frequency and corresponding mode shape of X-GPLRC spherical shell ($h/R = 0.05$, $\varphi_{in} = 15°$, $W_{GPL} = 0.5\%$ and $(K_w, K_g) = (0,0)$): (a) SS, (b) CC and (c) SF

References

Affdl, J.H. and Kardos, J.L. (1976), "The HalpinTsai equations: a review", *Polym. Eng. Sci.*, **16**(5), 344-352. https://doi.org/10.1002/pen.760160512.

Akbarov, S.D., Guliyev, H.H. and Yahnioglu, N. (2016), "Natural vibration of the three-layered solid sphere with middle layer made of FGM: three-dimensional approach", *Struct. Eng. Mech.*, **57**(2), 239-263. http://dx.doi.org/10.12989/sem.2016.57.2.239.

Anirudh, B., Ganapathi, M., Anant, C. and Polit, O. (2019), "A comprehensive analysis of porous graphene-reinforced curved beams by finite element approach using higher-order structural theory: Bending, vibration and buckling", *Compos. Struct.*, **222**, p.110899. https://doi.org/10.1016/j.compstruct.2019.110899.

Ansari, R., Torabi, J. and Shojaei, M.F. (2016), "Vibrational analysis of functionally graded carbon nanotube-reinforced composite spherical shells resting on elastic foundation using the variational differential quadrature method", *Eur. J. Mech. A-Solid.,* **60**, 166-182. https://doi.org/10.1016/j.euromechsol.2016.07.003.

Artioli, E. and Viola, E. (2005), "Static analysis of shear-deformable shells of revolution via GDQ method", *Struct. Eng. Mech.*, **19**(4), 459-475. https://doi.org/10.12989/sem.2005.19.4.459.

Artioli, E. and Viola, E. (2006), "Free vibration analysis of spherical caps using a GDQ numerical solution", *J. Press. Vess-T. Asme.*, **128**(3), 370-378. https://doi.org/10.1115/1.2217970.

Cadelano, E., Palla, P.L., Giordano, S. and Colombo, L., (2009), "Nonlinear elasticity of monolayer graphene", *Phys. Rev. Lett.*, **102**(23), p.235502. https://doi.org/10.1103/PhysRevLett.102.235502.

Chandra, Y., Chowdhury, R., Scarpa, F., Adhikari, S., Sienz, J., Arnold, C., Murmu, T. and Bould, D. (2012), "Vibration frequency of graphene based composites: a multiscale approach", *Mat. Sci. Eng. B-Adv.*, **177**(3), 303-310. https://doi.org/10.1016/j.mseb.2011.12.024.

Dong, Y.H., Zhu, B., Wang, Y., Li, Y.H. and Yang, J. (2018), "Nonlinear free vibration of graded graphene reinforced cylindrical shells: Effects of spinning motion and axial load", *J. Sound. Vib.*, **437**, 79-96. https://doi.org/10.1016/j.jsv.2018.08.036.

Dong, Y.H., Li, Y.H., Chen, D. and Yang, J. (2018), "Vibration characteristics of functionally graded graphene reinforced porous nanocomposite cylindrical shells with spinning motion", *Compos. Part. B-Eng.*, **145**, 1-13. https://doi.org/10.1016/j.compositesb.2018.03.009.

Feng, C., Kitipornchai, S. and Yang, J. (2017), "Nonlinear free vibration of functionally graded polymer composite beams reinforced with graphene nanoplatelets (GPLs)", *Eng. Struct.*, **140**, 110-119. https://doi.org/10.1016/j.engstruct.2017.02.052.

Gao, K., Gao, W., Chen, D. and Yang, J. (2018), "Nonlinear free vibration of functionally graded graphene platelets reinforced porous nanocomposite plates resting on elastic foundation", *Compos. Struct.*, **204**, 831-846. https://doi.org/10.1016/j.compstruct.2018.08.013.

Gholami, R. and Ansari, R. (2018), "Nonlinear harmonically excited vibration of third-order shear deformable functionally graded graphene platelet-reinforced composite rectangular plates", *Eng. Struct.*, **156**, 197-209. https://doi.org/10.1016/j.engstruct.2017.11.019.

Gholami, R. and Ansari, R. (2019), "Nonlinear stability and vibration of pre/post-buckled multilayer FG-GPLRPC rectangular plates", *Appl. Math. Model.*, **65**, 627-660. https://doi.org/10.1016/j.apm.2018.08.038.

Guo, H., Cao, S., Yang, T. and Chen, Y. (2018), "Vibration of laminated composite quadrilateral plates reinforced with graphene nanoplatelets using the element-free IMLS-Ritz method", *Int. J. Mech. Sci.*, **142**, 610-621. https://doi.org/10.1016/j.ijmecsci.2018.05.029.

Javani, M., Kiani, Y., Sadighi, M. and Eslami, M.R. (2019), "Nonlinear vibration behavior of rapidly heated temperature-dependent FGM shallow spherical shells", *AIAA. J.*, **57**(9), 4071-4084. https://doi.org/10.2514/1.J058240.

Kar, V.R. and Panda, S.K. (2015), "Nonlinear flexural vibration of shear deformable functionally graded spherical shell panel", *Steel. Compos. Struct.*, **18**(3), 693-709. https://doi.org/10.12989/scs.2015.18.3.693.

Kiani, Y. (2018), "Isogeometric large amplitude free vibration of graphene reinforced laminated plates in thermal environment using NURBS formulation", *Comput. Method. Appl. M.*, **332**, 86-101. https://doi.org/10.1016/j.cma.2017.12.015.

Kiani, Y. and Mirzaei, M. (2019), "Isogeometric thermal postbuckling of FG-GPLRC laminated plates", *Steel and Compos. Struct.*, **32**(6), 821-832. https://doi.org/10.12989/scs.2019.32.6.821.

Kitipornchai, S., Chen, D. and Yang, J. (2017), "Free vibration and elastic buckling of functionally graded porous beams reinforced by graphene platelets", *Mater. Design.*, **116**, 656-665. https://doi.org/10.1016/j.matdes.2016.12.061.

Kulkarni, Dhaval D., Ikjun Choi, Srikanth S. Singamaneni, and Vladimir V. Tsukruk. (2010) "Graphene oxide− polyelectrolyte nanomembranes", *ACS. Nano*., **4**(8) 4667-4676. https://doi.org/10.1021/nn101204d.

Liu, D., Kitipornchai, S., Chen, W. and Yang, J. (2018), "Three-dimensional buckling and free vibration analyses of initially stressed functionally graded graphene reinforced composite cylindrical shell", *Compos. Struct.*, **189**, 560-569. https://doi.org/10.1016/j.compstruct.2018.01.106.

Malekzadeh, P., Setoodeh, A.R. and Shojaee, M. (2018), "Vibration of FG-GPLs eccentric annular plates embedded in piezoelectric layers using a transformed differential quadrature method", *Comput. Method. Appl. M.*, **340**, 451-479. https://doi.org/10.1016/j.cma.2018.06.006.

Rafiee, M.A., Rafiee, J., Wang, Z., Song, H., Yu, Z.Z. and Koratkar, N. (2009), "Enhanced mechanical properties of nanocomposites at low graphene content", *ACS Nano.*, **3**(12), 3884-3890. https://doi.org/10.1021/nn9010472.

Reddy, C.D., Rajendran, S. and Liew, K.M. (2006), "Equilibrium configuration and continuum elastic properties of finite sized graphene", *Nanotechnology*, **17**(3), p.864. https://doi.org/10.1088/0957-4484/17/3/042.

Reddy, J.N. (2006), Theory and analysis of elastic plates and shells, *CRC press*.

Saidi, A.R., Bahaadini, R. and Majidi-Mozafari, K. (2019), "On vibration and stability analysis of porous plates reinforced by graphene platelets under aerodynamical loading", *Compos. Part. B-Eng.*, **164**, 778-799. https://doi.org/10.1016/j.compositesb.2019.01.074.

Scarpa, F., Adhikari, S. and Phani, A.S. (2009), "Effective elastic mechanical properties of single layer graphene sheets", *Nanotechnology*, **20**(6), p.065709.

Novoselov, K.S., Geim, A.K., Morozov, S.V., Jiang, D., Zhang, Y., Dubonos, S.V., Grigorieva, I.V. and Firsov, A.A. (2004), "Electric field effect in atomically thin carbon films", *Science*, **306**(5696), 666-669. https://doi.org/1126/science.1102896.

Potts, J.R., Dreyer, D.R., Bielawski, C.W. and Ruoff, R.S. (2011), "Graphene-based polymer nanocomposites", *Polymer*, **52**(1), 5-25. https://doi.org/10.1016/j.polymer.2010.11.042.

Qu, Y., Long, X., Yuan, G. and Meng, G. (2013), "A unified formulation for vibration analysis of functionally graded shells of revolution with arbitrary boundary conditions", *Compos. Part. B-Eng.*, **50**, 381-402. https://doi.org/10.1016/j.compositesb.2013.02.028.

Shen, H.S., Lin, F. and Xiang, Y. (2017), "Nonlinear vibration of functionally graded graphene-reinforced composite laminated beams resting on elastic foundations in thermal environments", *Nonlinear. Dynam.*, **90**(2), 899-914. https://doi.org/10.1007/s11071-017-3701-0.

Shen, H.S., Xiang, Y. and Fan, Y., (2019), "Nonlinear vibration of thermally postbuckled FG-GRC laminated beams resting on elastic foundations", *Int. J. Struct. Stab. Dy.*, **25**(9), 1507-1520. https://doi.org/10.1142/S0219455419500512.

Shen, H.S., Xiang, Y. and Fan, Y. (2019), "Vibration of thermally postbuckled FG-GRC laminated plates resting on elastic foundations", *J. Vib. Control.*, **19**(6), p.1950051. https://doi.org/10.1177/1077546319825671.

Shen, H.S., Xiang, Y. and Lin, F. (2017), "Nonlinear vibration of functionally graded graphene-reinforced composite laminated plates in thermal environments", *Comput. Method. Appl. M.*, **319**, 175-193. https://doi.org/10.1016/j.cma.2017.02.029.

Shen, H.S., Xiang, Y. and Fan, Y. (2017), "Nonlinear vibration of functionally graded graphene-reinforced composite laminated cylindrical shells in thermal environments", *Compos. Struct.*, **182**, 447-456. https://doi.org/10.1016/j.compstruct.2017.09.010.

Shen, H.S., Xiang, Y., Fan, Y. and Hui, D. (2018), "Nonlinear vibration of functionally graded graphene-reinforced composite laminated cylindrical panels resting on elastic foundations in thermal environments", *Compos. Part. B-Eng.*, **136**, 177-186. https://doi.org/10.1016/j.compositesb.2017.10.032.

Song, M., Kitipornchai, S. and Yang, J. (2017), "Free and forced vibrations of functionally graded polymer composite plates reinforced with graphene nanoplatelets", *Compos. Struct.*, **159**, 579-588. https://doi.org/10.1016/j.compstruct.2016.09.070.

Stankovich, S., Dikin, D.A., Dommett, G.H., Kohlhaas, K.M., Zimney, E.J., Stach, E.A., Piner, R.D., Nguyen, S.T. and Ruoff, R.S. (2006), "Graphene-based composite materials", *Nature*, **442**(7100), p.282. https://doi.org/10.1038/nature04969

Thai, C.H., Ferreira, A.J.M., Tran, T.D. and Phung-Van, P. (2019), "Free vibration, buckling and bending analyses of multilayer functionally graded graphene nanoplatelets reinforced composite plates using the NURBS formulation", *Compos. Struct.*, **220**, 749-759. https://doi.org/10.1016/j.compstruct.2019.03.100.

Tornabene, F. and Viola, E. (2007), "Vibration analysis of spherical structural elements using the GDQ method", *Comput. Math. Appl.*, **53**(10), 1538-1560. https://doi.org/10.1016/j.camwa.2006.03.039.

Wang, M., Xu, Y.G., Qiao, P. and Li, Z.M. (2019), "A two-dimensional elasticity model for bending and free vibration analysis of laminated graphene-reinforced composite beams", *Compos. Struct.*, **211**, 364-375. https://doi.org/10.1016/j.compstruct.2018.12.033.

Wang, Y., Xie, K., Fu, T. and Shi, C. (2019), "Vibration response of a functionally graded graphene nanoplatelet reinforced composite beam under two successive moving masses", *Compos. Struct.*, **209**, 928-939. https://doi.org/10.1016/j.compstruct.2018.11.014.

Wang, A., Chen, H., Hao, Y. and Zhang, W. (2018), "Vibration and bending behavior of functionally graded nanocomposite doubly-curved shallow shells reinforced by graphene nanoplatelets", *Results. Phys.*, **9**, 550-559. https://doi.org/10.1016/j.rinp.2018.02.062.

Wu, H., Kitipornchai, S. and Yang, J. (2017), "Thermal buckling and postbuckling of functionally graded graphene nanocomposite plates", *Mater. Design.*, **132,** 430-441. https://doi.org/10.1016/j.matdes.2017.07.025.

Zhang, Y.Y., Wang, C.M., Cheng, Y. and Xiang, Y. (2011), "Mechanical properties of bilayer graphene sheets coupled by sp3 bonding", *Carbon*, **49**(13), 4511-4517. https://doi.org/10.1016/j.carbon.2011.06.058.

Zhao, X., Zhang, Q., Chen, D. and Lu, P. (2010), "Enhanced mechanical properties of graphene-based poly (vinyl alcohol) composites", *Macromolecules*, **43**(5), 2357-2363. https://doi.org/10.1021/ma902862u.

Zhao, Z., Feng, C., Wang, Y. and Yang, J. (2017), "Bending and vibration analysis of functionally graded trapezoidal nanocomposite plates reinforced with graphene nanoplatelets (GPLs)", *Compos. Struct.*, **180**, 799-808. https://doi.org/10.1016/j.compstruct.2017.08.044.

CC